THE JOURNAL OF PHYSICAL CHEMISTRY A
A JOURNAL OF THE AMERICAN CHEMICAL SOCIETY

pubs.acs.org/JPCA Article

# Seeded Crystal Growth of Internally Mixed Organic–Inorganic Aerosols: Impact of Organic Phase State

Shuichi B. Ushijima, Erik Huynh, Ryan D. Davis,* and Margaret A. Tolbert*

Cite This: J. Phys. Chem. A 2021, 125, 8668–8679 Read Online

ACCESS | Metrics & More | Article Recommendations | Supporting Information

**ABSTRACT:** Atmospheric aerosols are complex with both inorganic and organic components. The soluble inorganics can transition between aqueous and crystalline phases through efflorescence and deliquescence. This study focuses on the efflorescence of $(NH_4)_2SO_4$/organic particles by seeded crystal growth through contact with a crystal of $(NH_4)_2SO_4$. Seeded crystal growth is known to effectively shut down supersaturation of aqueous aerosols. Here, we investigate whether organics can inhibit seeded crystal growth. We demonstrate that poly(ethylene glycol) 400 (PEG-400), which phase-separates from the aqueous $(NH_4)_2SO_4$ and forms a core–shell structure, did not inhibit seeded crystal growth of $(NH_4)_2SO_4$ at all relative humidity (RH) values below deliquescence RH. The PEG-400 layer was not viscous enough to prevent the diffusion of species through the coating. In contrast, we find that although raffinose, which stays homogeneously mixed with $(NH_4)_2SO_4$, did not inhibit seeded crystal growth at RH > 45%, it did inhibit heterogeneous efflorescence at lower humidities. Viscosity measurements using an electrodynamic balance show a significant increase in viscosity as humidity was lowered, suggesting that inhibited diffusion of water and ions prevented efflorescence. The observed efflorescence at the higher RH also demonstrates that collisions can induce efflorescence of mixed aerosols that would otherwise not homogeneously effloresce.

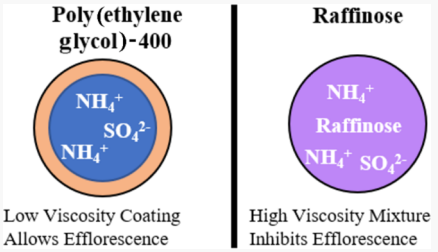


## 1. INTRODUCTION

Atmospheric aerosols can be found in various phase states including liquid, solid, and glass depending on temperature and relative humidity (RH).[1−4] For soluble inorganic salts, an aqueous liquid droplet loses water to the surrounding air and crystallizes, or effloresces, at a specific relative humidity termed the efflorescence relative humidity (ERH). The reverse process where a salt crystal absorbs water from the surrounding air to form an aqueous droplet is called deliquescence, which occurs at the deliquescence relative humidity (DRH). While the DRH is thermodynamically determined, it is difficult to predict the ERH due to kinetic barriers to nucleation.[5] Thus, efflorescence typically occurs at a lower relative humidity (RH) than deliquescence, allowing salt solutions to be supersaturated under many atmospheric conditions. While the homogeneous phase transitions for salts have been studied in detail,[5] heterogeneous efflorescence has yet to be fully examined.

Heterogeneous immersion efflorescence is initiated by an insoluble particle inside an aqueous droplet that induces crystallization from within. In heterogeneous contact efflorescence, a nucleus collides with the aqueous droplet and induces efflorescence from the exterior surface of the droplet. The presence of the heterogeneous nucleus, at the surface or inside the aqueous droplet, has been shown to lower the kinetic barrier to nucleation and is experimentally observed as an increase in the ERH.[6−9] The degree to which the ERH is increased depends on the aqueous droplet's composition and the identity of the heterogeneous nucleus.[6−9] In a study where the supersaturated salt solutions were contacted with a solid crystal of the same salt, seeded crystal growth eliminates the need for nucleation and efflorescence occurs at an RH very near the DRH, effectively shutting down hysteresis.[6] While seeded crystal growth has been observed for several inorganic droplets,[6] it is not clear if such a mechanism would be viable for more complex droplets of atmospheric relevance composed of inorganic/organic mixtures.

Organic aerosols typically do not crystallize but remain liquid or amorphous even when the humidity and or temperature has been lowered.[10,11] Laboratory studies where soluble inorganics were mixed with organic molecules have shown that some organics will inhibit efflorescence by lowering the ERH value when compared to the pure inorganic droplet[12] or can even prevent efflorescence all together.[13] Further, as some organic aerosols are dried and/or cooled, they transition into a glassy particle.[11] Glasses are particles with an amorphous structure whose viscosities have become high enough that they are essentially solid.[14] The temperature and humidity conditions necessary for an organic molecule to transition into a glass are different for each organic. While laboratory studies measuring the viscosity of secondary organic aerosol

Received: May 20, 2021
Published: September 23, 2021







https://doi.org/10.1021/acs.jpca.1c04471
J. Phys. Chem. A 2021, 125, 8668–8679

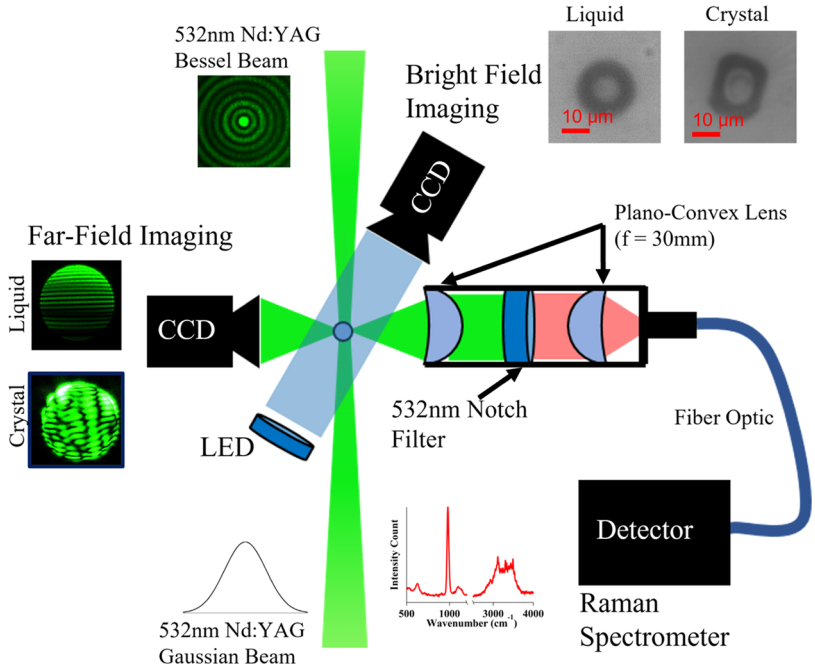


**Figure 1.** Arrangement of CCD cameras and LED to observe and record far-field and bright-field scattering. Arrangement of lenses, notch filter, and fiber optic to obtain a Raman spectrum of levitated droplet is also shown. Sample images of a liquid and crystal particle for far-field and bright-field are shown. A sample Raman spectrum is also shown. The beam profiles of the trapping lasers are shown. The beam from above has a Bessel profile, while the beam from below has a Gaussian profile.

(SOA) from different precursors have been conducted,[15,16] the diversity of SOA compounds has made it difficult to fully characterize their impacts. Models that estimate the glass transition of a compound have been suggested based on molecular characteristics such as the atomic O/C ratio and molar mass.[17,18] In the atmosphere where the temperatures are colder than earth's surface, some studies have suggested that organic glasses are more common, especially in the middle to upper troposphere.[11,19]

When considering efflorescence of mixed organic/inorganic droplets, the mixing state could be an important factor. For example, for some organics, liquid−liquid phase separation (LLPS) can result in an organic coating around an aqueous inorganic core, but other organics may only partially engulf the inorganic core.[20−22] Studies have shown that the O/C ratio, along with water activity, can be used as a predictor for morphology.[21] The aerosol pH has also been shown to affect the separation RH for LLPS formation.[22] More viscous organics may promote glass formation.[15,17] The mixing state and phase state of complex aerosols are important factors that determine their impact on climate through direct effects but also indirect effects such as cloud aerosol interactions.[1,2,23] Studies have shown that crystalline salts and sea spray aerosols can act as heterogeneous ice nuclei, suggesting their involvement in ice cloud formation.[24,25] Studies examining the impact of organics on cloud formation have shown that organic liquid droplets and solid glasses can act as contact ice nuclei.[26] Additionally, long-chain alcohols have been shown to catalyze the freezing of inorganic solutions.[27] Understanding how organics influence the phase state of inorganic aerosols can further our understanding of the complex aerosol−cloud interactions impacting climate.

Here, we examined the effect of two different model organics, raffinose and poly(ethylene glycol) 400 (PEG-400), on the efflorescence behavior of $(NH_4)_2SO_4$. Specifically, we probed whether the two organics would inhibit seeded crystal growth of the $(NH_4)_2SO_4$ fraction when contacted with a crystal of $(NH_4)_2SO_4$. Raffinose is a trisaccharide that has been detected in atmospheric aerosols[28] and has a high glass-transition temperature ($T_g$ = 397.5 K),[11] allowing pure raffinose to form a glass at room temperature when dried. PEG-400 is a polymer whose average molecular weight is 400 amu and can also be described as a polyol. Polyols are organic molecules containing multiple hydroxy groups, which have been detected in atmospheric aerosols.[28] PEG-400 was specifically chosen due to it undergoing LLPS with $(NH_4)_2SO_4$ at a 1:1 weight ratio below 90% RH.[29] We use an optical trap to examine if either of these organics, when mixed 1:1 with ammonium sulfate, will inhibit efflorescence of ammonium sulfate by seeded crystal growth. Complementary measurements using an electrodynamic balance (EDB) technique were used to determine the viscosity of the mixed particles with raffinose as a function of RH.

## 2. METHODS

**2.1. Preparation of Droplets and Contact Nuclei.** To generate organic/inorganic droplets, solutions of 5 wt % total of 1:1 $(NH_4)_2SO_4$/raffinose and $(NH_4)_2SO_4$/PEG-400 in high-performance liquid chromatography (HPLC) grade water (Sigma-Aldrich) were prepared. Purely inorganic or organic droplets were generated similarly by creating a 5 wt % solution of either $(NH_4)_2SO_4$, PEG-400, or raffinose in HPLC grade water. $(NH_4)_2SO_4$, D-(+)-raffinose pentahydrate, and PEG-400 were all obtained from Sigma-Aldrich. The solutions were filtered through a nylon filter with 0.45 $\mu$m pores. A droplet generator (Microfab MJ-APB-20) was used to create droplets by applying an alternating positive and negative voltage to a piezoelectric ring near the tip of a glass capillary with a 20 $\mu$m diameter orifice.


https://doi.org/10.1021/acs.jpca.1c04471
J. Phys. Chem. A 2021, 125, 8668−8679

Droplets are trapped inside a rectangular flow cell with observational windows on all four sides. To control and measure the RH inside the flow cell, two $N_{2(g)}$ flows are used. One flows directly into a mass flow controller, while the other passes through a water bubbler filled with HPLC water to humidify the flow before going to a mass flow controller. The two flows then are mixed and enter the flow cell from below the trapping site and exit above the trapping site. Two probes (Vaisala HMP60) are placed at the inlet and outlet of the flow cell to measure RH. The RH at the trapping region is calculated as the average of the two probes (±1 standard deviation (SD)).

Heterogeneous nuclei of $(NH_4)_2SO_4$ crystals are generated by diverting the dry flow after the mass flow controller toward a nebulizer (Omron NE-U22). The nebulizer is filled with 3−4 mL of a solution of 10 wt % $(NH_4)_2SO_4$ and creates droplets of the solution. The droplets are carried into a diffusion drier causing efflorescence of the $(NH_4)_2SO_4$ (ERH = 35%). The gas carrying the particles of crystalline $(NH_4)_2SO_4$ then mixes with the wet flow before entering the flow cell. The time for the $(NH_4)_2SO_4$ particles to transit from the nebulizer to the observation cell is approximately 5 min at a total flow rate of 15 sccm. Long retention times of several hours have been shown to allow $(NH_4)_2SO_4$ to transition from spherical to rectangular morphologies.[30] Due to our short transit times, we expect most of the seed particles to be spherical in morphology. Adsorption of water onto inorganic aerosols below their DRH has also been shown to influence their surface properties.[31] In this study, we were not able to directly determine the water adsorption or the crystal morphology, and thus their impact on the seeded crystal growth is unclear.

**2.2. Optical Trapping and Raman Spectroscopy.** Figure 1 depicts the optical trapping setup inside the flow cell.[32] Two counterpropagating 532 nm Nd:YAG lasers enter above and below the droplet. The laser from below has a Gaussian profile with a beamwidth of approximately 300 $\mu$m. The wide beam profile increases the probability of a droplet falling into the beam path and becoming trapped. However, due to the wide beam profile, the trap from the Gaussian beam alone is not axially robust. Thus, to enhance droplet trapping, a Bessel beam with a narrow central core (∼15 $\mu$m) illuminates the droplet from above. The trapped droplet is observed by two charge-coupled device (CCD) cameras that are placed perpendicular to the laser axis. One of the cameras takes images of far-field scattering, while the other obtains bright-field microscopy images using a light-emitting diode (LED) to illuminate the particle. By adjusting the camera to focus on the scattered light from the droplet, near-field scattering can also be imaged onto the CCD cameras. Near-field scattering, as shown in previous studies using the optical levitator, can be used to detect collisions between the levitated droplet and heterogeneous nuclei.[31] However, due to the limited number of cameras, seeded crystal growth experiments were run with only far-field and bright-field microscopies. Near-field imaging was used to determine the collision rate.

Raman spectroscopy has been coupled to the optical levitator to obtain chemical information about the trapped droplet. The light scattered by the aerosol from the trapping lasers is collected and collimated by a plano-convex lens with a focal length of 30 mm. The collimated light is filtered through a 532 nm notch filter to remove the Rayleigh scattering and allow the Raman signal to pass. The light is then focused onto a fiber-optic cable with another plano-convex lens, which carries the signal to a Raman detector (Teledyne Princeton Instruments FERGIE). The lenses, filter, and fiber-optic adaptor are joined by a cage system to form a single optical assembly. The position of the joined optical assembly can be adjusted in all three directions to maximize the signal collected from the droplet. The spectra are collected at 1 s exposures per frame, with each spectrum made up of 120 frames that are averaged. Spectra are reported over the relative wavenumber range of 500−4000 $cm^{-1}$. To minimize stray light from entering the detector, a black covering for the optical assembly was applied. Additionally, a curtain is drawn over the entire laser table and the laboratory's lights are turned off during acquisition to limit ambient light from entering the detector.

**2.3. Observing Efflorescence.** Efflorescence of the droplet can be determined by observing the far-field scattering pattern. As shown in Figure 1, the far-field scattering pattern is distinctly different for a liquid droplet vs a crystalline particle. Because the liquid droplet is spherical, Mie scattering is observed as alternating bright and dark bands, which are stable for constant RH and thus size. The crystal, however, scatters light differently and, due to the multitude of crystal facets, creates a mosaic pattern that changes in time as the crystal rotates inside the trap. The bright-field microscopy images of the trapped aerosol can also yield information about the shape of the droplet and thus efflorescence. Example far-field and bright-field images of a liquid and a crystal from the present study are included in Figure 1. The liquid is shown to be spherical with a Mie scattering pattern in the far-field, while the crystal has a rectangular prism shape and a mosaic scattering pattern in the far-field. While the crystal can have a nonspherical or spherical morphology, inhomogeneities in the bright-field image, due to light passing through the crystal facets, can be used to determine efflorescence.

**2.4. Experimental Protocol for Seeded Crystal Growth Experiments.** To observe seeded crystal growth, a droplet of the $(NH_4)_2SO_4$/organic solution is trapped in the flow cell. The trapped droplet is exposed to a particle stream of crystalline $(NH_4)_2SO_4$ for a maximum of 25 s at a set RH. The rate of collision was determined by counting the number of contact events observed in near-field scattering imaging for a trapped droplet exposed to a stream of crystalline $(NH_4)_2SO_4$. It was found that the trapped droplet encounters approximately six collisions on average (from eight trials) within a 25 s exposure period for a collision rate of 0.24 collisions·$s^{-1}$. The video of the far-field images from the CCD cameras was monitored during the exposure period to determine whether the droplet effloresced during the exposure period. If the droplet did not effloresce, the droplet was ejected from the trap and a new droplet was captured for a new trial. The process was repeated at different RH values to calculate a probability of efflorescence ($P_{Eff}$) as the ratio of observed efflorescence events to the number of total trials as a function of RH. For each RH range, a total of four to five experiments were conducted. In addition to the probability of efflorescence, the average number of collisions needed to induce efflorescence was calculated. For this, the exposure time needed to induce efflorescence was multiplied by an average collision rate of 0.24 collisions·$s^{-1}$.

**2.5. Measuring Viscosity and Immersion Times.** The viscosity of $(NH_4)_2SO_4$/raffinose droplets and the immersion time scales for $(NH_4)_2SO_4$ crystals into PEG-400 droplets were studied in a dual-balance linear quadrupole electrodynamic balance (DBQ-EDB), as described extensively


https://doi.org/10.1021/acs.jpca.1c04471
J. Phys. Chem. A 2021, 125, 8668−8679

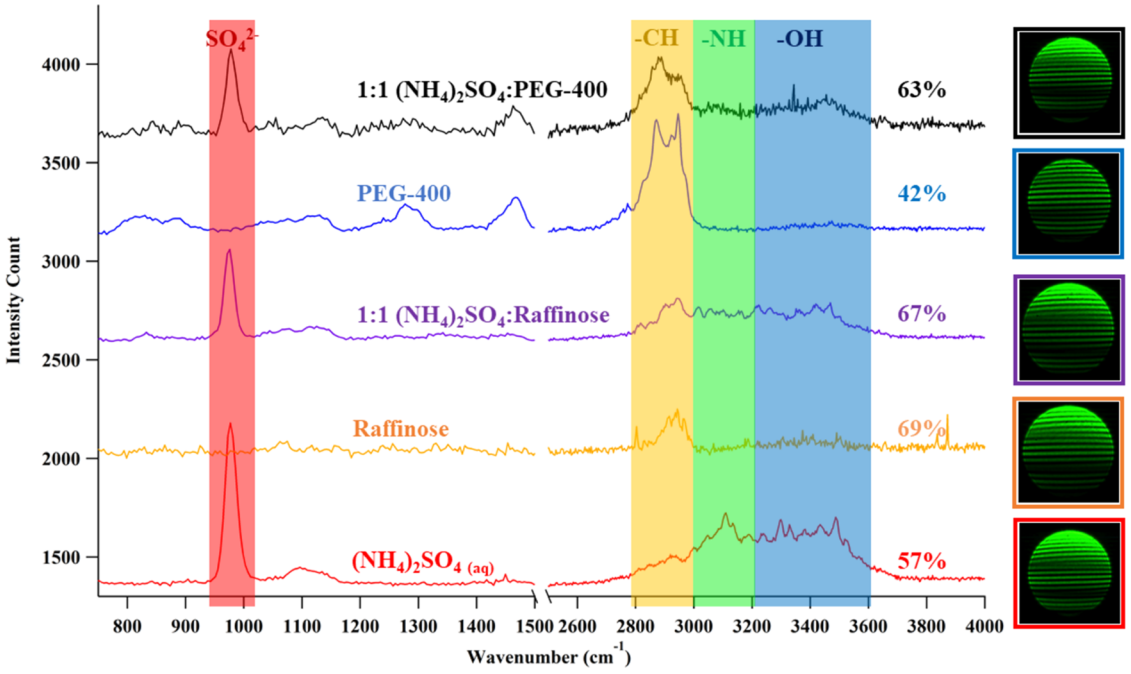


**Figure 2.** Raman spectra of $(NH_4)_2SO_4$ (red), raffinose (yellow), 1:1 $(NH_4)_2SO_4$/raffinose (purple), PEG-400 (blue), and 1:1 $(NH_4)_2SO_4$/PEG-400 (black). The two mixtures are 1:1 by weight. For each spectrum, the RH and scattering image of the droplet is shown to the right. The relevant peaks have been highlighted with colors. The $SO_4^{2-}$ (red) is a sharp peak at ∼980 $cm^{-1}$, the organic −CH (yellow) is a broad peak below 3000 $cm^{-1}$, the −NH (green) is a broad peak centered at ∼3100 $cm^{-1}$, and the −OH (blue) is a broad peak centered at ∼3500 $cm^{-1}$.

elsewhere[33] and shown in Figure S1 in the Supporting Information. In the DBQ-EDB technique, two particles can be simultaneously levitated and equilibrated at the same RH and then subsequently merged to infer viscosity and other physical characteristics of the merged particles. As shown in Figure S1a, droplets are generated from 5 wt % stock solutions using piezo-driven droplet dispensers (50 $\mu$m orifice; Micro-Fab) and injected into the DBQ-EDB through an induction electrode, which charges the surface of the droplets. In the DBQ-EDB, the linear quadrupole, with an applied oscillating voltage ($V_{ac}$ ±600 V at 300 Hz typical), axially confines the charged droplets. Two independent counterbalance electrodes ($V_{dc}$ ±200 V typical) counter the force of gravity and the drag force from a humidified nitrogen gas flow (which controls the RH within the DBQ-EDB). The levitated particles are oppositely charged, with the particle in the bottom balance having a higher net charge. When the voltage from the top balance is removed, the two particles merge through electrostatic attraction and the morphology of the merged dimer is tracked as a function of time using far-field laser scatter and bright-field imaging, as seen in Figure S1a.

Once two $(NH_4)_2SO_4$/raffinose droplets are caught in the trap, the droplets are allowed to equilibrate with the RH for 30 min before merging. Upon merging of two viscous liquid droplets, the merged dimer exponentially relaxes to a spherical shape to minimize surface energy. The time it takes to relax to sphericity is related to the viscosity ($\eta$), surface tension ($\sigma$), and density of the merged droplets, as well as the radius ($r$) of the relaxed sphere.[33,34] Above viscosities of ∼40 mPa·s, such as the case in the present study (where the lower limit to our measurements is limited by camera imaging frame rate within our experimental setup), merged droplets are in the over-damped regime where the characteristic time scale of coalescence ($\tau$) can be related to viscosity through eq 1

$$\tau \approx \frac{\eta r}{\sigma} \tag{1}$$

where $\tau$ is measured from an exponential fit to the relaxation of dimer aspect ratio (in bright-field images) or far-field defect image correlation values.[32,33] With this measured $\tau$, viscosity can be calculated using the above equation. For the calculations, $\sigma$ was approximated as 55 ± 30 $mN{\cdot}m^{-1}$ and $r$ = 18 ± 2 $\mu$m.[33]

The DBQ-EDB technique was also used to provide insight into the factors influencing the movement of crystalline $(NH_4)_2SO_4$ through liquid PEG-400. Thus, as shown in Figure S1b, a 15 $\mu$m diameter crystalline $(NH_4)_2SO_4$ particle was merged with a 30 $\mu$m diameter PEG-400 droplet at 30% RH. The particles used in these experiments are much larger than those used for crystal seeded growth in the optical levitator, which provides insight into the relative importance of diffusion at the moment of contact between liquid PEG-400 and crystalline $(NH_4)_2SO_4$.

## 3. RESULTS

**3.1. Raman Characterization of Trapped Internally Mixed Droplets.** Figure 2 shows Raman spectra taken in the optical levitator for droplets of aqueous $(NH_4)_2SO_4$, raffinose, PEG-400, 1:1 $(NH_4)_2SO_4$/raffinose, and $(NH_4)_2SO_4$/PEG-400. For each droplet, the far-field scattering is shown to the right indicating that each is spherical. As seen in the figure, a sharp peak at ∼980 $cm^{-1}$ for $SO_4^{2-}$ and a broad peak centered at ∼3100 $cm^{-1}$ for −NH are observed for the three droplets containing $(NH_4)_2SO_4$. A broad peak below 3000 $cm^{-1}$ indicates organics for all of the droplets that contain raffinose or PEG-400. Finally, a broad peak centered at ∼3500 $cm^{-1}$ indicates −OH for water. From the spectra, it is clear that the droplets prepared to be mixtures do indeed contain both ammonium sulfate and the organic of interest, indicating we


https://doi.org/10.1021/acs.jpca.1c04471
J. Phys. Chem. A 2021, 125, 8668−8679

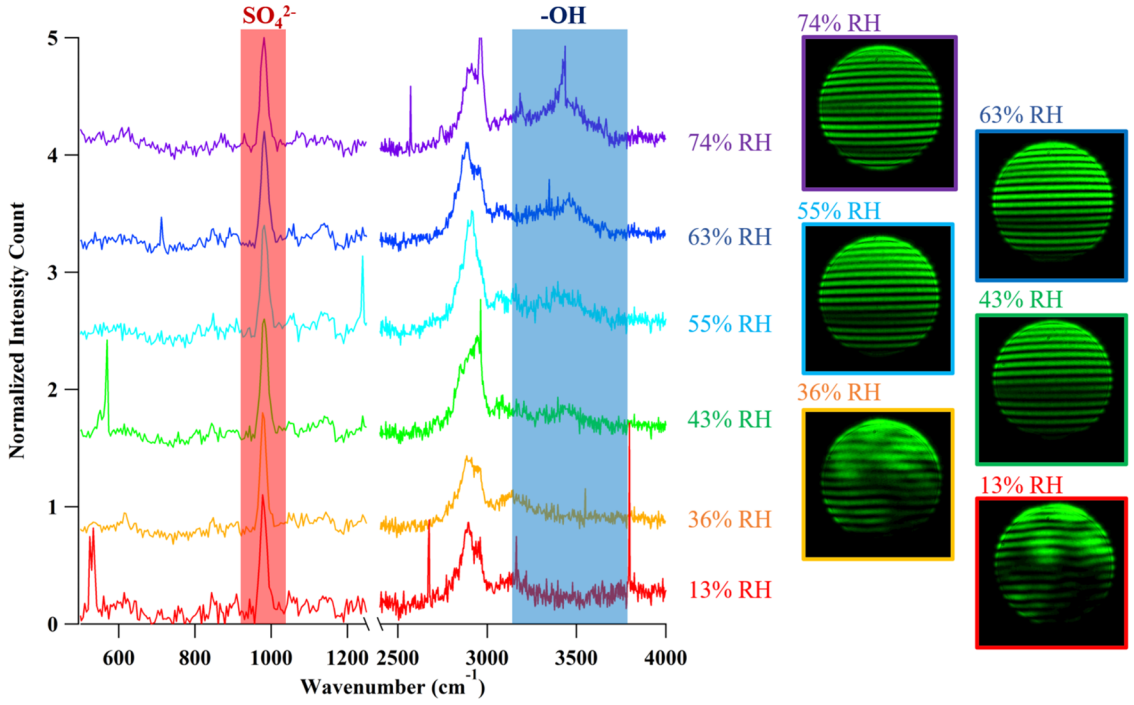


**Figure 3.** Spectra and scattering images for dehumidification of 1:1 $(NH_4)_2SO_4$/PEG-400. The droplet began at 74% RH and was lowered to 13% RH. The spectra have been normalized to the $SO_4^{2-}$ peak and offset from each other. The $SO_4^{2-}$ (red) peak at ∼980 $cm^{-1}$ and −OH (blue) broad peak centered at ∼3500 $cm^{-1}$ are highlighted. The sharp peaks seen near 2600 and 3500 $cm^{-1}$ at 74% RH and 2700 and 3800 $cm^{-1}$ at 13% RH are likely due to cosmic ray radiation.

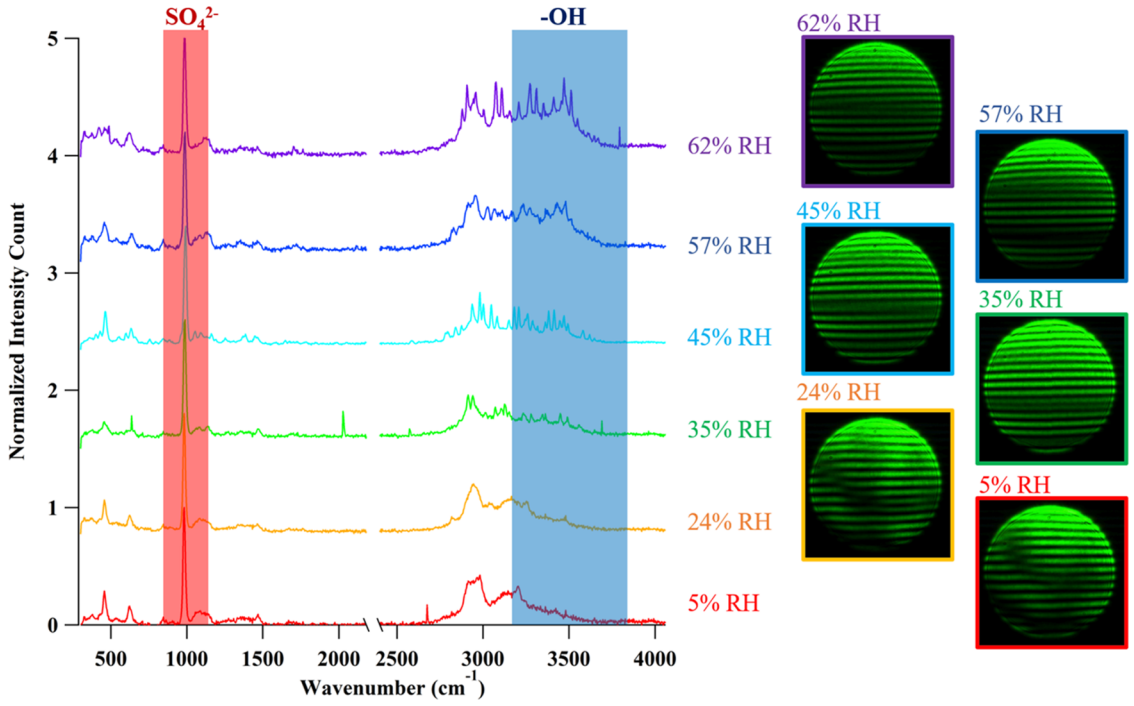


**Figure 4.** Spectra and scattering images for an efflorescence experiment on 1:1 $(NH_4)_2SO_4$/raffinose by weight. The droplet began at 62% RH and was lowered to 15% RH. The spectra have been normalized to the $SO_4^{2-}$ peak and offset from each other. The $SO_4^{2-}$ (red) peak at ∼980 $cm^{-1}$ and the −OH (blue) broad peak centered at ∼3500 $cm^{-1}$ are highlighted.

are creating an internally mixed composition droplet. In Figure 2, the −OH peak did not appear strongly for the PEG-400 and the raffinose droplets used in the figure, most likely due to showing all of the spectra in one plot. Figures S2 and S3 in the Supporting Information show expanded views of the spectra of PEG-400 and raffinose at various RH, and it can be seen that −OH-related peaks do appear for PEG-400 at ∼42% and for raffinose at ∼70% RH.

**3.2. Homogeneous Efflorescence of Mixed $(NH_4)_2SO_4$/Organic Droplets.** A series of spectra and far-field scattering



https://doi.org/10.1021/acs.jpca.1c04471
J. Phys. Chem. A 2021, 125, 8668−8679

images for a dehumidification experiment of 1:1 $(NH_4)_2SO_4$/PEG-400 are shown in Figure 3. The droplet was first captured at ~74% RH, and the RH was gradually lowered to 13% RH (see Figure S4 in the Supporting Information for RH experimental trajectory). The droplet undergoes efflorescence at 36% RH as seen by the change in the far-field scattering patterns at 43 and 36% RH. The scattering pattern at and below 36% RH consists of horizontal lines with major interferences contorting the lines, suggesting some combination of sphericity and rigidity. Since PEG-400 remains liquid at room temperature and does not crystallize (see Figure S2 in the Supporting Information), the rigidity is likely due to the effloresced $(NH_4)_2SO_4$ crystal. We believe the scattering pattern is due to the liquid PEG-400 coating the crystallized $(NH_4)_2SO_4$ particle. While we cannot confirm whether the coating creates a core−shell or partially engulfed structure, a study on 1:1 $(NH_4)_2SO_4$/PEG-400 droplets on a plate shows PEG-400 coating $(NH_4)_2SO_4$ before and after efflorescence.[29] The pattern also resembles the scattering image of an aqueous droplet with mineral dust particles immersed inside taken from the previous work in the optical levitator.[7] The Raman spectra also show the change in droplet composition with RH. As the droplet is dried and loses water to the surrounding, the −OH peak becomes less intense. For the effloresced particle at 36% RH, the −OH signal is near zero, consistent with crystallization of the aqueous core. Upon efflorescence of $(NH_4)_2SO_4$, the $SO_4^{2-}$ peak has been shown to shift to a lower wavenumber and become narrower.[35] As shown in Figure S5 of the Supporting Information, the $SO_4^{2-}$ peak does seem to shift to a lower wavenumber for the $(NH_4)_2SO_4$/PEG-400 particle below 36%, providing additional evidence that the $(NH_4)_2SO_4$ has effloresced. Our resolution is not sufficient to observe any potential peak narrowing upon efflorescence. The observed homogeneous ERH of a 1:1 $(NH_4)_2SO_4$/PEG-400 and the Raman spectra are also consistent with other studies that investigated this mixture using a droplet on a plate technique, which found a homogeneous ERH of 33 ± 4% RH.[29] The observed ERH of the mixed aerosol is also consistent with the homogeneous ERH of pure $(NH_4)_2SO_4$ near 35% RH.[5]

Figure 4 shows data for a similar experiment with a droplet of 1:1 $(NH_4)_2SO_4$/raffinose. In this experiment, the droplet was first captured at 62% RH and was dried to 5% RH. While pure raffinose, like PEG-400, does not crystallize upon drying below the homogeneous ERH of $(NH_4)_2SO_4$[13] (also see Figure S3 in the Supporting Information), it seems to inhibit efflorescence of $(NH_4)_2SO_4$ when mixed. The efflorescence inhibition at room temperature is consistent with a previous study done on 1:1 $(NH_4)_2SO_4$/raffinose droplets observed previously.[13] As seen by the scattering images, the linear Mie scattering pattern remains even as the humidity is lowered to single-digit values well below the homogeneous ERH of pure $(NH_4)_2SO_4$. There are some interferences to Mie scattering at low RH, which could potentially be localized regions of inhomogeneities impacting the refractive index. A study on a droplet of $(NH_4)_2SO_4$ mixed with sucrose, a disaccharide formed from two of the three monosaccharides that make up raffinose, in an EDB coupled with Raman microscopy, showed that under dry conditions an enhancement of sucrose was observed near the surface of the droplet.[36] If raffinose were to respond similarly at low RH, the enhancement at the surface can create differences in refractive index within the droplet causing the observed interferences to the Mie scattering. Additionally, the inorganic ions and raffinose may be interacting to form a gel-like state.[37] Since gels are a liquid within a porous solid network, this may cause nonuniform density and refractive index and thus slight disruptions in the Mie scattering. Despite the slight disruptions in Mie fringes at low RH, the scattering is more consistent with an amorphous phase formed through gradual loss of water upon decreasing RH. The Raman spectra are also consistent with the gradual loss of water indicated by the slowly decreasing −OH signal as the droplet is dried. Note, however, in contrast to the PEG-400 system, water is still present in the droplet at 5% RH.

Homogeneous efflorescence was further probed using a self-correlation technique to analyze the far-field images and calculate a defect intensity as a function of time as discussed previously in Davis et al.[32] Briefly, self-correlation is achieved by making a copy of the far-field image, shifting it 20 pixels to the right and calculating the defect as the absolute difference between the original and the shifted images. For Mie scattering of a spherical particle, indicating either a liquid or amorphous particle, the intensity is relatively constant in the horizontal direction and thus the shifting does not cause a high defect value. However, for a crystalline particle, the mosaic pattern causes the shifted image to be significantly different from the original, leading to a high defect value. Figure 5 shows a plot of defect intensity vs time for a droplet of $(NH_4)_2SO_4$/PEG-400 undergoing homogeneous efflorescence at 34.9% RH and a droplet of $(NH_4)_2SO_4$/raffinose at 4.7% RH. For the droplet with PEG-400, the defect intensity is low until the droplet undergoes efflorescence near 15 s when the defect intensity increases significantly. The defect is highest right after efflorescence due to the change in trapping position. As the droplet settles in the new trap position, the defect stabilizes at a higher value than before efflorescence. For the droplet with raffinose, the defect intensity at 4.7% RH remains constant and low, indicating that it has not effloresced despite the droplet being dried to well below the homogeneous ERH of pure $(NH_4)_2SO_4$.

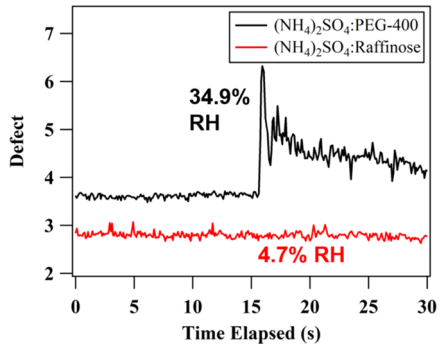


**Figure 5.** Plot of defect intensity with the elapsed time for homogeneous efflorescence of a 1:1 $(NH_4)_2SO_4$/PEG-400 at 34.9% RH and a droplet of 1:1 $(NH_4)_2SO_4$/raffinose at 4.7% RH.

**3.3. Seeded Crystal Growth of Mixed $(NH_4)_2SO_4$/Organic Droplets.** Seeded crystal growth experiments for $(NH_4)_2SO_4$/PEG-400 were conducted at RH values ranging from 41.6 and 82.9% RH. Experiments below 41.6% RH were not performed because the mixed droplet homogeneously effloresces at 36% RH. For droplets of $(NH_4)_2SO_4$/raffinose, seeded crystal growth was studied for RH values ranging from 16.9 to 84.2% RH. Figure 6 shows three sample seeded crystal growth experiments: one at a high RH for a mixed droplet of


https://doi.org/10.1021/acs.jpca.1c04471
J. Phys. Chem. A 2021, 125, 8668−8679

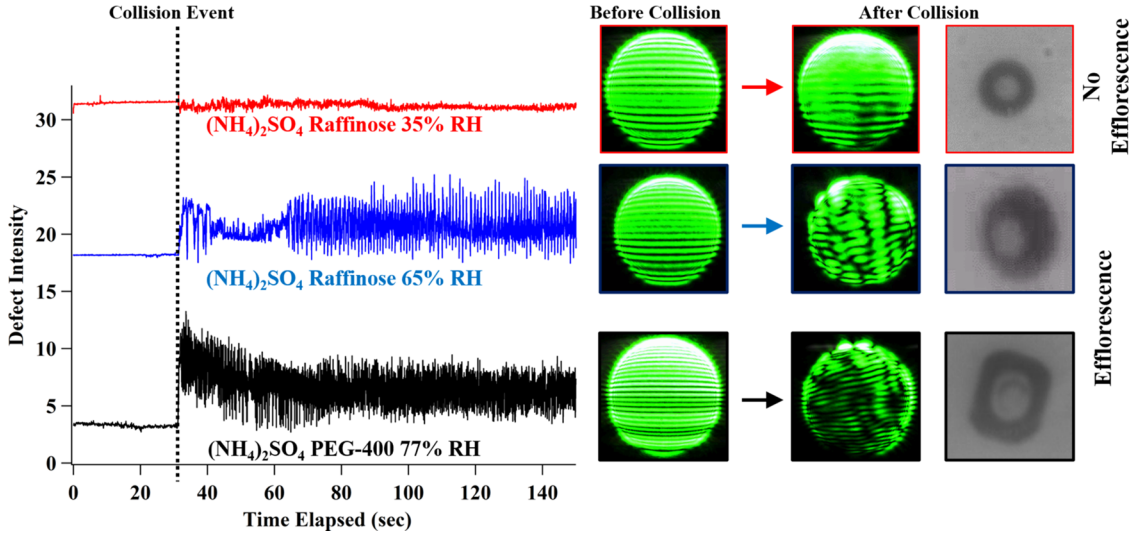


**Figure 6.** Defect intensity with time elapsed for three seeded crystal growth experiments. Two experiments are shown with 1:1 $(NH_4)_2SO_4$/raffinose at 35 and 65% RH. The third experiment is for 1:1 $(NH_4)_2SO_4$/PEG-400 at 77% RH. The collision event, which causes significant change to the defect intensity, has been shown as the dotted line on the graph. For each contact experiment, the scattering image for the droplet before and after the collisions is shown. The bright-field image of the droplet after the collisions is also shown.

$(NH_4)_2SO_4$/PEG-400 and two for mixed droplets with raffinose at two different RH values with two differing results. For each experiment, a plot of the defect intensity with elapsed time is shown. The plots have been aligned at the collision event, as determined by a significant change to the far-field image. Far-field scattering images before and after the collision, as well as the bright-field image after the collision, are also shown. In the experiment with $(NH_4)_2SO_4$/PEG-400 at 77% RH, it can be seen that the defect intensity is at a stable and low value before the collision, but upon collision, it increases rapidly and then stabilizes at a higher level. The variance in defect also increases greatly after the collision. The far-field scattering pattern changes upon collision, and the bright-field image of the droplet after collision indicates a rectangular prism shape. The rigid shape of the particle is most likely due to the crystallized $(NH_4)_2SO_4$ core. As shown in previous seeded crystal growth experiments with $(NH_4)_2SO_4$, when the crystallization RH was above 69% RH, the crystal formed a rectangular prism.[32] All of these criteria indicate that the droplet effloresced rapidly upon collision. For the experiment with $(NH_4)_2SO_4$/raffinose at 65% RH, similar results are observed. Upon collision, the defect increases, the far-field scattering loses the Mie scattering pattern, and the bright-field image of the crystal is less spherical, all indicating efflorescence. In contrast, the experiment shown for $(NH_4)_2SO_4$/raffinose at 35% RH has a different outcome. Upon collision, the defect intensity does not rapidly increase although the variance in the data increases. While there are interferences to the far-field scattering image, it still maintains the Mie scattering pattern, which suggests that the particle maintains a spherical shape. The interference is believed to be due to the colliding crystal of $(NH_4)_2SO_4$ adhering to the surface without causing efflorescence of the droplet. The spherical bright-field image after collision further supports our belief that the heterogeneous nucleus did not induce efflorescence.

Seeded crystal growth experiments were repeated for both organic mixtures over a range of RH values, and a summary of the results is shown in Figure 7. The homogeneous ERH and DRH of pure $(NH_4)_2SO_4$ are shown as vertical dashed lines for

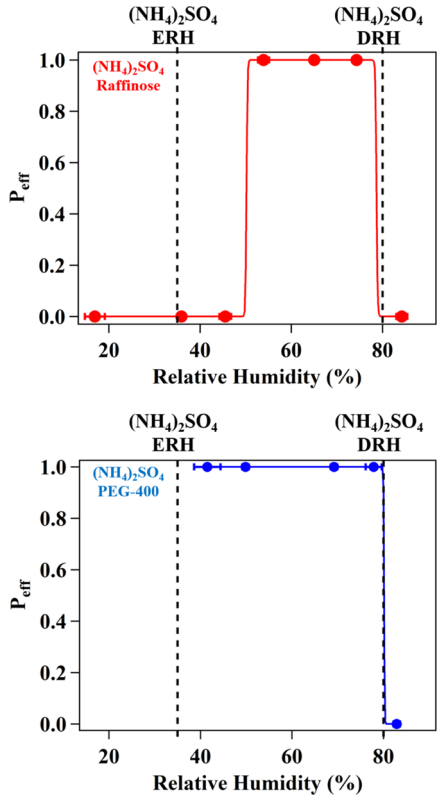


**Figure 7.** Summary of results for the seeded crystal growth of 1:1 $(NH_4)_2SO_4$/raffinose (top) or 1:1 $(NH_4)_2SO_4$/PEG-400 (bottom) by a crystal of $(NH_4)_2SO_4$.

reference. For both mixed droplets, no efflorescence was observed ($P_{Eff}$ = 0) above the homogeneous DRH of $(NH_4)_2SO_4$ at 80% RH. This result is expected as the thermodynamically favored state above 80% RH is the aqueous solution of $(NH_4)_2SO_4$. For every RH tested between the DRH and ERH of $(NH_4)_2SO_4$, the droplets mixed with PEG-400 effloresced upon contact with $P_{Eff}$ = 1. As seen on the plot, the highest RH that efflorescence was observed for the


https://doi.org/10.1021/acs.jpca.1c04471
J. Phys. Chem. A 2021, 125, 8668−8679

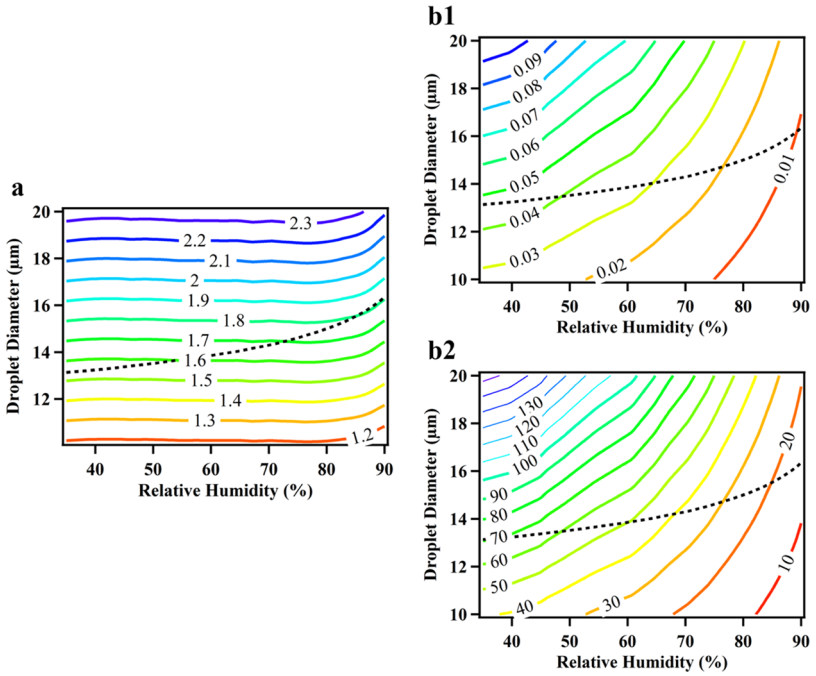


**Figure 8.** (a) Plot of the calculated thickness of the PEG-400 coating (in $\mu$m) as a function of droplet diameter and RH. Calculated diffusion times (in seconds) for a molecule of $H_2O$ (b1) or a heterogeneous nucleus that is 300 nm in diameter (b2) as a function of droplet diameter and RH. The dotted line represents the change in droplet diameter and coating thickness or diffusion times for a droplet that begins as a 15 $\mu$m droplet at 80% RH as RH is changed.

$(NH_4)_2SO_4$/PEG-400 droplet was 77.8 ± 1.8% RH. The result is consistent with the seeded crystal growth of pure $(NH_4)_2SO_4$ droplets by crystals of itself,[6] suggesting that the PEG-400 coating had minimal effect on the seeded crystal growth of the aqueous core. The behavior of the $(NH_4)_2SO_4$/raffinose mixtures below 80% RH was similar to that of $(NH_4)_2SO_4$/PEG-400 until the RH was lowered to 45.5 ± 1.3% RH. For experiments conducted at and below 45.5 ± 1.3% RH, no efflorescence was observed upon contact ($P_{Eff}$ = 0). Figure S6 in the Supporting Information shows the average number of collisions needed to induce efflorescence as a function of RH for those experiments where efflorescence was observed. It can be seen that most experiments that resulted in efflorescence required between one and two collisions.

## 4. DISCUSSION

### 4.1. Internally Mixed Ammonium Sulfate/PEG-400.

To determine why the PEG-400 coating did not affect the seeded crystal growth, the diffusion times through the coating were estimated. Figure 8a shows the estimated thickness of the PEG-400 coating in $\mu$m as a function of the droplet's diameter (core plus coating) and humidity. To calculate the thickness, it was assumed that all of the $(NH_4)_2SO_4$ is in the aqueous core and all of the PEG-400 is in the organic coating. The assumption is not perfect as a study of a 1:1 $(NH_4)_2SO_4$/PEG-400 droplet on a plate showed that small satellites of aqueous $(NH_4)_2SO_4$ are contained in the PEG-400 coating.[29] However, due to a lack of quantitative data on the satellites, they were not included. Additionally, it was assumed that the concentration of $(NH_4)_2SO_4$ in the aqueous portion was determined by the RH. This assumption was based on the observation that the homogeneous ERH of the $(NH_4)_2SO_4$/PEG-400 matched that of pure $(NH_4)_2SO_4$. The density and water content of $(NH_4)_2SO_4$ as a function of RH were obtained through the E-AIM model.[38] For PEG-400, water content as a function of RH was obtained from Marcolli and Krieger,[39] and densities as a function of mole fraction of PEG-400 in water were obtained from Han et al.[40] A detailed description of the calculation is provided in the Supporting Information. The black dotted line in Figure 8 represents an example trajectory for a droplet that begins as a 15 $\mu$m droplet at 80% RH as the humidity is decreased. As the droplet dries, the overall diameter decreases while the organic layer's thickness also thins. The decrease in size and thickness of the droplet and organic coating is due to both $(NH_4)_2SO_4$ and PEG-400 responding to changes in RH. Over the course of an experiment, the organic coating decreases from around 1.8 to 1.5 $\mu$m as humidity decreases from 80 to 40% RH.

Based on the estimated thickness of the PEG-400 layer, diffusion times through the layer for a molecule of $H_2O$ (Figure 8b1) with a molecular diameter of 2.75 Å and a heterogeneous nucleus with a diameter of 300 nm (Figure 8b2) were calculated. The heterogeneous nucleus size was based on the size distribution of the crystalline $(NH_4)_2SO_4$ measured in an SMPS (TSI 3010). The distribution is included as Figure S7 in the Supporting Information and shows that the mode diameter is approximately 300 nm. The diffusion time ($\tau$) was calculated as

$$\tau = \frac{X^2}{2D} \tag{2}$$

where $X$ is the organic layer's thickness, and $D$ is the diffusion coefficient ($cm^2 \cdot s^{-1}$). The diffusion coefficient for a molecule or particle traveling through the PEG-400 layer can be estimated as

$$D = \frac{k_B T}{6\pi\eta r} \tag{3}$$



https://doi.org/10.1021/acs.jpca.1c04471
J. Phys. Chem. A 2021, 125, 8668−8679

where $k_B$ is the Boltzmann constant ($1.381 \times 10^{-23}$ J·K$^{-1}$), $T$ is temperature (K), $\eta$ is the viscosity of the PEG-400 coating (Pa·s), and $r$ is the radius of the diffusing molecule or particle. The viscosity of PEG-400 as a function of mole fraction of PEG-400 in water was obtained from Jerome et al.[41] A plot of PEG-400 viscosity as a function of RH and the resulting diffusion coefficients for a water molecule and a 300 nm heterogeneous nucleus are shown in Figure S8 in the Supporting Information. As seen in Figure 8b1, it takes a fraction of a second for water to travel through the PEG-400 layer under our experimental conditions. The rapid diffusion time for a molecule of water suggests that the coating of PEG-400 is not viscous enough to prevent water from leaving the aqueous core upon efflorescence and thus does not inhibit efflorescence of $(NH_4)_2SO_4$. The diffusion times for a heterogeneous nucleus such as the crystalline particles of $(NH_4)_2SO_4$ to travel from the outside to the inner core are much slower, taking tens of seconds to approximately 2 min. This time scale is longer than the experimental observation of seconds for the droplet of $(NH_4)_2SO_4$/PEG-400 to effloresce upon collision.

To understand the discrepancy, we measured the time scale for a crystal of $(NH_4)_2SO_4$ of ∼15 μm in diameter to become completely immersed into a droplet of PEG-400 that is ∼30 μm in diameter at 30% RH in the DBQ-EDB. As shown in Figure S1b, it took the crystal less than 0.1 s to become fully submerged into the PEG-400, suggesting that forces other than diffusion can cause the heterogeneous nucleus to become immersed into the PEG-400 layer and reach the $(NH_4)_2SO_4$ core. Forces such as convection within the droplet created by the air flowing around the droplet or capillary forces between the particle and the PEG-400 could be responsible for carrying the heterogeneous nucleus to the $(NH_4)_2SO_4$ faster than by diffusion alone. Additionally, the satellite pockets of aqueous $(NH_4)_2SO_4$ that are dispersed throughout the PEG-400 layer could also play a role in crystallization. For example, the crystalline $(NH_4)_2SO_4$ seed could encounter a satellite first, causing it to crystallize, which then continues to crystallize the remainder of the aqueous portion.

**4.2. Internally Mixed Ammonium Sulfate/Raffinose.** Raffinose inhibited the effloresce of $(NH_4)_2SO_4$ both homogeneously and during seeded crystallization at low RH. Previous studies have shown that the viscosity of pure raffinose increases as humidity is lowered.[42] Specifically, the viscosity of pure raffinose increases an order of magnitude for every 5% decrease in RH (see Figure S9 in the Supporting Information) to a point that at ∼40% RH the viscosity was too high for an accurate measurement to be made.[42] Here, the viscosity of a 1:1 mixture of $(NH_4)_2SO_4$/raffinose was determined in the DBQ-EDB by measuring the coalescence time for two droplets of 1:1 $(NH_4)_2SO_4$/raffinose to merge into one droplet. The results for the viscosities as a function of RH are plotted in Figure 9. The viscosities were also extrapolated up to 100% RH. Based on the fit, the diffusion coefficient for molecules of $H_2O$ and $SO_4^{2-}$ (ionic radius = 0.242 nm[43]) was determined and is also included in Figure 9. We note that at low water activity and high viscosity, the Stokes−Einstein relationship may underpredict the diffusion of water,[44] and thus the values shown here likely represent the lower limit on $D$ and thus an upper limit on time scales. The diffusion coefficient for $NH_4^+$ is not shown since its ionic radius (0.154 nm[45]) is smaller than $SO_4^{2-}$ and thus $SO_4^{2-}$ diffuses slower and would be the limiting factor to crystallization. As shown in Figure 9, when the mixed droplet reaches an RH of 35%, the homogeneous

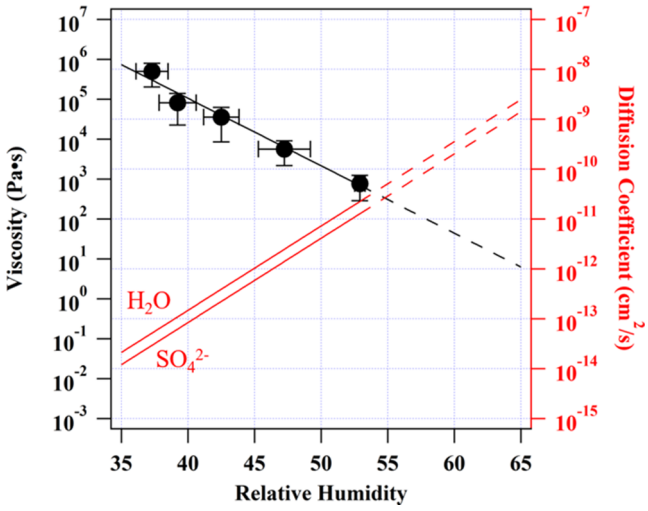


**Figure 9.** Measured viscosities of 1:1 $(NH_4)_2SO_4$/raffinose droplets at various RH values. Diffusion coefficients for molecules of $H_2O$ and $SO_4^{2-}$ traveling through the mixture at various RH values are shown on the right axis.

ERH of $(NH_4)_2SO_4$, the viscosity has already reached $10^6$ Pa·s. The high viscosity prevents the $(NH_4)_2SO_4$ from crystallizing at 35% RH, and thus the 1:1 $(NH_4)_2SO_4$/raffinose aerosol does not effloresce homogeneously at room temperature.

Seeded crystal growth experiments showed that the mixed droplet of $(NH_4)_2SO_4$/raffinose began resisting crystallization between 45.5 ± 1.3 and 53.9 ± 1.2% RH. The viscosities at 45.5 and 53.9% RH are $1.2 \times 10^4$ and 450 Pa·s, respectively, which suggests that the viscosity threshold necessary for a droplet to undergo efflorescence is somewhere between those limits. Calculated diffusion times are shown in Table 1 for a

**Table 1. Diffusion Times for a $H_2O$ Molecule and a $SO_4^{2-}$ Ion Traveling 1 or 7.5 μm through a Droplet of 1:1 $(NH_4)_2SO_4$/Raffinose at 45.5% and 53.9% RH**

| | 45.5% RH $1.2 \times 10^4$ Pa·s | | 53.9% RH 450 Pa·s | |
|---|---|---|---|---|
| | $H_2O$ | $SO_4^{2-}$ | $H_2O$ | $SO_4^{2-}$ |
| $D$ (cm$^2$·s$^{-1}$) | $1.3 \times 10^{-12}$ | $7.4 \times 10^{-13}$ | $3.4 \times 10^{-11}$ | $1.9 \times 10^{-11}$ |
| $\tau$ (1 μm) | 1.1 h | 1.9 h | 2.5 min | 4.4 min |
| $\tau$ (7.5 μm) | ∼60 h | ∼106 h | 2.3 h | 4.1 h |

molecule of $H_2O$ and an ion of $SO_4^{2-}$ to diffuse distances of 7.5 and 1 μm in a droplet of 1:1 $(NH_4)_2SO_4$/raffinose at 45.5 and 53.9% RH, respectively. The 7.5 μm distance represents the time it takes the molecule to travel out from the center of a droplet that is 15 μm in diameter. The 1 μm diffusion time represents the time for the molecules and ions to move through the outermost layer of the droplet. Efflorescence is initiated by the movement of ions from the aqueous to crystalline phase, followed by loss of the water that had been solvating the ions. However, as seen in the table for the droplet of 1:1 $(NH_4)_2SO_4$/raffinose, movement of ions and water is significantly hindered at 45.5% RH. For a water molecule to travel 1 μm, it would take approximately 1 h and approximately 2.5 days to travel through 7.5 μm. The viscosity is thus too high for ions to diffuse to the heterogeneous nucleus and for water to evaporate out of the droplet, thus inhibiting efflorescence. For the droplet at 53.9% RH where seeded crystal growth was observed, the times for $H_2O$ to travel 1 and


https://doi.org/10.1021/acs.jpca.1c04471
J. Phys. Chem. A 2021, 125, 8668−8679

7.5 $\mu$m are 2.5 min and 2.3 h, respectively. Based on diffusion times, water near the surface of the droplet could evaporate and cause efflorescence, while the water near the center of the droplet probably could not. The surface enhancement of sucrose for a mixed particle of sucrose and $(NH_4)_2SO_4$ observed in a study by Chu and Chan[36] could be a similar phenomenon, where the surface has lost water, creating a crust-like feature and trapping the components in the interior of the particle.

**4.3. Limitations of the Present Study to Atmospheric Conditions.** Secondary organic aerosols and inorganic aerosols such as $(NH_4)_2SO_4$ have been found together in the atmosphere in significant amounts by in situ measurements.[46] Over terrestrial regions, $(NH_4)_2SO_4$ is one of the predominant inorganic species and internally mixed aerosols of $(NH_4)_2SO_4$/organic droplets are expected to be found. Seeded crystal growth of such aerosols can occur when two plumes with different RH histories mix at RH conditions between the ERH and DRH of $(NH_4)_2SO_4$. If one of the plumes had come from RH conditions that were low enough to effloresce $(NH_4)_2SO_4$, these crystals could act as seed crystals for the internally mixed aerosols. While calculating the exact number of these specific collisions is beyond the scope of this work, future studies using realistic particle composition and concentration could elucidate the importance of contact in atmospheric phase changes.

Our present study examined how efflorescence is strongly affected by changes in viscosity due to changes in RH at room temperature. However, atmospheric conditions are much colder, and it has been shown that glass formation and viscosity of organic species are affected greatly by temperature.[19,47] In general, organics tend to be more viscous at lower temperatures and thus we expect as conditions get colder, organics will inhibit efflorescence of $(NH_4)_2SO_4$ at higher RH than found in this room-temperature study. Low temperatures can also affect the phase state of the soluble inorganic.[48−50] For example, the tetrahydrate of $(NH_4)_2SO_4$ is believed to form under ice-saturating conditions below 220 K.[48] Additionally, NaCl dihydrate has been shown to form at temperatures below ~250 K.[49,50] The different inorganic phases can have different ice-nucleating characteristics, changing their impact on climate.[49,50] The effect of temperature, specifically low temperatures, on the phase state of aerosols is important, and further studies should be conducted to further understand the efflorescence of particles in the atmosphere.

## 5. CONCLUSIONS

Internally mixed aerosols composed of both organic and inorganic aerosols are commonly believed to be in the liquid state due to the incorporation of the organic fraction. The assumption has been revisited as studies on organic glasses,[11−19,42] inorganic gels,[37] and heterogeneous efflorescence of aerosols[6−9] have shown other processes that can influence the phase state of the aerosol. In this study, we examined the effect of organics on the efflorescence of $(NH_4)_2SO_4$ by mixing with two model organics: PEG-400 and raffinose. PEG-400 phase-separates from the aqueous $(NH_4)_2SO_4$ and creates an organic coating. Raffinose can transition into a glass at room temperature upon lowering the RH. By contacting these mixed droplets with a crystal of $(NH_4)_2SO_4$, the study showed that viscosity is more important than the morphology of the mixed droplet. The organic coating of PEG-400 seemed to have little to no effect on the efflorescence of $(NH_4)_2SO_4$. By calculating the thickness of the coating and using measured viscosities of PEG-400 from the literature, we showed that the organic coating does not act as a barrier for the transfer of water molecules out from the aqueous core at room temperature. Additionally, the PEG-400 coating also allowed a heterogeneous nucleus to pass through with ease, allowing heterogeneous efflorescence to occur. Unless the heterogeneous nucleus is chemically transformed by the interaction with the organic layer, it is unlikely that an LLPS aerosol whose outer coating is not highly viscous will have any effect on homogeneous or heterogeneous efflorescence. Raffinose, on the other hand, was highly effective at inhibiting the efflorescence of $(NH_4)_2SO_4$. The glassy organic caused the viscosity of the mixed aerosol to be highly sensitive to RH, where an ~10% RH difference would result in changes to the diffusion coefficient and diffusion times by ~2 orders of magnitude. In the middle and upper tropospheres where aerosols are believed to be mostly glassy,[19] homogeneous and heterogeneous efflorescence are likely to have little impact. However, in the lower troposphere where the aerosol phase will be based on RH,[19] homogeneous and heterogeneous efflorescence can still be a major process affecting the phase state of aerosols.

## ■ ASSOCIATED CONTENT

### Supporting Information

The Supporting Information is available free of charge at https://pubs.acs.org/doi/10.1021/acs.jpca.1c04471.

Explanation of how the PEG-400-coating thickness was calculated for various droplet diameters and RH (Section 1); overview of the experiment for merging droplets in dual-balance linear quadrupole electrodynamic balance (DBQ-EDB) to measure viscosity (Figure S1a); description of methods for measuring immersion times of $(NH_4)_2SO_4$ crystals into droplets of PEG-400 (Figure S1b); Raman spectra and far-field images of PEG-400 at various RH (Figure S2); Raman spectra and far-field images of raffinose at various RH (Figure S3); sample RH trajectory for typical homogeneous efflorescence experiment (Figure S4); Raman spectra of $(NH_4)_2SO_4$/PEG-400 homogeneous efflorescence, focused on the $SO_4^{2-}$ peak (Figure S5); average number of collisions needed to induce efflorescence as a function of RH (Figure S6); size distribution of the heterogeneous nucleus composed of crystalline $(NH_4)_2SO_4$ (Figure S7); viscosity of PEG-400 and the calculated diffusion coefficient as a function of RH (Figure S8); viscosity vs RH for pure raffinose and 1:1 $(NH_4)_2SO_4$/raffinose (Figure S9) (PDF)

## ■ AUTHOR INFORMATION


### Corresponding Authors

**Ryan D. Davis** − *Department of Chemistry, Trinity University, San Antonio, Texas 78212, United States;* orcid.org/0000-0002-4434-1320; Phone: (210) 999-7827; Email: rdavis5@trinity.edu

**Margaret A. Tolbert** − *Department of Chemistry, University of Colorado, Boulder, Boulder, Colorado 80309, United States; Cooperative Institute for Research in Environmental Science, University of Colorado, Boulder, Boulder, Colorado 80309, United States;* Phone: (303) 492-3179; Email: margaret.tolbert@colorado.edu




https://doi.org/10.1021/acs.jpca.1c04471
J. Phys. Chem. A 2021, 125, 8668−8679

## Authors

**Shuichi B. Ushijima** − *Department of Chemistry, University of Colorado, Boulder, Boulder, Colorado 80309, United States; Cooperative Institute for Research in Environmental Science, University of Colorado, Boulder, Boulder, Colorado 80309, United States;* orcid.org/0000-0002-9536-2295

**Erik Huynh** − *Department of Chemistry, Trinity University, San Antonio, Texas 78212, United States*

Complete contact information is available at: https://pubs.acs.org/10.1021/acs.jpca.1c04471


## Notes

The authors declare no competing financial interest.

## ■ ACKNOWLEDGMENTS

This material is based upon the work supported by the National Science Foundation under Grant Number AGS1925191. Any opinions, findings, and conclusions or recommendations expressed in this material are those of the author(s) and do not necessarily reflect the view of the National Science Foundation. This work was also supported by NASA Headquarters under the NASA Earth and Space Science Fellowship Program, Grant "80NSSC17K0655".

## ■ REFERENCES


(1) Seinfeld, J. H.; Pandis, S. N. *Atmospheric Chemistry and Physics*, 2nd ed.; Wiley-Interscience: Hoboken, NJ, 2006.

(2) Andreae, M. O.; Rosenfeld, D. Aerosol-Cloud-Precipitation Interactions. Part 1. The Nature and Sources of Cloud-Active Aerosols. *Earth-Sci. Rev.* **2008**, *89*, 13−41.

(3) Boucher, O.; Randall, D.; Artaxo, P.; Bretherton, C.; Feingold, G.; Forster, P.; Kerminen, V. M.; Kondo, Y.; Liao, H.; Lohmann, U.; Rasch, P. et al. Clouds and Aerosols. In *Climate Change 2013: The Physical Science Basis. Contribution of Working Group I to the Fifth Assessment Report of the Intergovernmental Panel on Climate Change*; Stocker, T. F.; Qin, D.; Plattner, G. K.; Tignor, M.; Allen, S. K.; Boschung, J.; Nauels, A.; Xia, Y.; Bex, V.; Midgley, P. M., Eds.; Cambridge University Press: Cambridge, U.K., 2013.

(4) Ramanathan, V.; Crutzen, P. J.; Kiehl, J. T.; Rosenfeld, D. Aerosols, Climate, and the Hydrological Cycle. *Science* **2001**, *294*, 2119−2124.

(5) Martin, S. T. Phase Transitions of Aqueous Atmospheric Particles. *Chem. Rev.* **2000**, *100*, 3403−3453.

(6) Davis, R. D.; Lance, S.; Gordon, J. A.; Ushijima, S. B.; Tolbert, M. A. Contact Efflorescence as a Pathway for Crystallization of Atmospherically Relevant Particles. *Proc. Natl. Acad. Sci. U.S.A.* **2015**, *112*, 15815−15820.

(7) Ushijima, S. B.; Davis, R. D.; Tolbert, M. A. Immersion and Contact Efflorescence Induced by Mineral Dust Particles. *J. Phys. Chem. A* **2018**, *122*, 1303−1311.

(8) Davis, R. D.; Tolbert, M. A. Crystal Nucleation Initiated by Transient Ion-Surface Interactions at Aerosol Interfaces. *Sci. Adv.* **2017**, *3*, No. e1700425.

(9) Martin, S. T.; Han, J.-H.; Hung, H.-M. The Size Effect of Hematite and Corundum Inclusions on the Efflorescence Relative Humidities of Aqueous Ammonium Sulfate Particles. *Geophys. Res. Lett.* **2001**, *28*, 2601−2604.

(10) Marcolli, C.; Luo, B.; Peter, T. Mixing of the Organic Aerosol Fractions: Liquids as the Thermodynamically Stable Phases. *J. Phys. Chem. A* **2004**, *108*, 2216−2224.

(11) Zobrist, B.; Marcolli, C.; Pedernera, D. A.; Koop, T. Do Atmospheric Aerosols Form Glasses? *Atmos. Chem. Phys.* **2008**, *8*, 5221−5224.

(12) Bodsworth, A.; Zobrist, B.; Bertram, A. K. Inhibition of Efflorescence in Mixed Organic-Inorganic Particles at Temperatures less than 250K. *Phys. Chem. Chem. Phys.* **2010**, *12*, 12259−12266.

(13) Robinson, C. B.; Schill, G. P.; Tolbert, M. A. Optical Growth of Highly Viscous Organic/Sulfate Particles. *J. Atmos. Chem.* **2014**, *71*, 145−156.

(14) Angell, C. A. Formation of Glasses from Liquids and Biopolymers. *Science* **1995**, *267*, 1924−1935.

(15) Petters, S. S.; Kreidenweis, S. M.; Grieshop, A. P.; Ziemann, P. J.; Petters, M. D. Temperature- and Humidity-Dependent Phase States of Secondary Organic Aerosols. *Geophys. Res. Lett.* **2019**, *46*, 1005−1013.

(16) Grayson, J. W.; Zhang, Y.; Mutzel, A.; Renbaum-Wolff, L.; Böge, O.; Kamal, S.; Herrmann, H.; Martin, S. T.; Bertram, A. Effect of Varying Experimental Conditions on the Viscosity of $\alpha$-pinene Derived Secondary Organic Material. *Atmos. Chem. Phys.* **2016**, *16*, 6027−6040.

(17) Koop, T.; Bookhold, J.; Shiraiwa, M.; Pöschl, U. Glass Transition and Phase State of Organic Compounds: Dependency on Molecular Properties and Implications for Secondary Organic Aerosol in the Atmosphere. *Phys. Chem. Chem. Phys.* **2011**, *13*, 19238−19255.

(18) DeRieux, W.-S. W.; Li, Y.; Lin, P.; Laskin, J.; Laskin, A.; Bertram, A. K.; Nizkorodov, S. A.; Shiraiwa, M. Predicting the Glass Transition Temperature and Viscosity of Secondary Organic Material using Molecular Composition. *Atmos. Chem. Phys.* **2018**, *18*, 6331−6351.

(19) Shiraiwa, M.; Li, Y.; Tsimpidi, A. P.; Karydis, V. A.; Berkemeier, T.; Pandis, S. N.; Lelieveld, J.; Koop, T.; Pöschl, U. Global Distribution of Particle Phase State in Atmospheric Secondary Organic Aerosols. *Nat. Commun.* **2017**, *8*, No. 15002.

(20) Freedman, M. A. Phase Separation in Organic Aerosol. *Chem. Soc. Rev.* **2017**, *46*, 7694−7695.

(21) Gorkowski, K.; Donahue, N. M.; Sullivan, R. C. Aerosol Optical Tweezers Constrain the Morphology Evolution of Liquid-Liquid Phase-Separated Atmospheric Particles. *Chem* **2020**, *6*, 204−220.

(22) Losey, D. J.; Parker, R. G.; Freedman, M. A. pH Dependance of Liquid-Liquid Phase Separation in Organic Aerosol. *J. Phys. Chem. Lett.* **2016**, *7*, 3861−3865.

(23) Riemer, N.; Ault, A. P.; West, M.; Craing, R. L.; Curtis, J. H. Aerosol Mixing State: Measurements, Modeling, and Impacts. *Rev. Geophys.* **2019**, *57*, 187−249.

(24) Niehaus, J.; Cantrell, W. Contact Freezing of Water by Salts. *J. Phys. Chem. Lett.* **2015**, *6*, 3490−3495.

(25) Demott, P. J.; Hill, T. C. J.; McCluskey, C. S.; Prather, K. A.; Collins, D. B.; Sullivan, R. C.; Ruppel, M. J.; Mason, R. H.; Irish, V. E.; Lee, T.; et al. Sea Spray Aerosol as a Unique Source of Ice Nucleating Particles. *Proc. Natl. Acad. Sci. U.S.A.* **2016**, *113*, 5797−5803.

(26) Collier, K. N.; Brooks, S. D. Role of Organic Hydrocarbons in Atmospheric Ice Formation via Contact Freezing. *J. Phys. Chem. A* **2016**, *120*, 10169−10180.

(27) Cantrell, W.; Robinson, C. Heterogeneous Freezing of Ammonium Sulfate and Sodium Chloride Solutions by Long Chain Alcohols. *Geophys. Res. Lett.* **2006**, *33*, No. L07802.

(28) Wan, E. C. H.; Yu, J. Z. Analysis of Sugars and Sugar Polyols in Atmospheric Aerosols by Chloride Attachment in Liquid Chromatography/Negative Ion Electrospray Mass Spectrometry. *Environ. Sci. Technol.* **2007**, *41*, 2459−2466.

(29) Ciobanu, V. G.; Marcolli, C.; Krieger, U. K.; Zuend, A.; Peter, T. Efflorescence of Ammonium Sulfate and Coated Ammonium Sulfate Particles: Evidence for Surface Nucleation. *J. Phys. Chem. A* **2010**, *114*, 9486−9495.

(30) Ueda, S. Morphological Change of Solid Ammonium Sulfate Particles below the Deliquescence Relative Humidity: Experimental Reproduction of Atmospheric Sulfate Particle Shapes. *Aerosol Sci. Technol.* **2021**, *55*, 423−437.

(31) Lin, J. J.; Raj, R. K.; Wang, S.; Kokkonen, E.; Mikkelä, M.-H.; Urpelainen, S.; Prisle, N. L. Pre-Deliquescent Water Uptake in Deposited Nanoparticles Observed with in Situ Ambient Pressure X-ray Photoelectron Spectroscopy. *Atmos. Chem. Phys.* **2021**, *21*, 4709−4727.

(32) Davis, R. D.; Lance, S.; Gordon, J. A.; Tolbert, M. A. Long Working-Distance Optical Trap for in Situ Analysis of Contact-Induced Phase Transformation. *Anal. Chem.* **2015**, *87*, 6186−6194.
(33) Richards, D.; Trobaugh, K.; Hajek-Herrera, J.; Davis, R. Dual-Balance Electrodynamic Trap as a Microanalytical Tool for Identifying Gel Transitions and Viscous Properties of Levitated Aerosol Particles. *Anal. Chem.* **2020**, *92*, 3086−3094.
(34) Song, Y.; Haddrell, A.; Bzdek, B.; Reid, J.; Bannan, T.; Topping, D.; Percival, C.; Cai, C. Measurements and Predictions of Binary Component Aerosol Particle Viscosity. *J. Phys. Chem. A* **2016**, *120*, 8123−8137.
(35) Yeung, M. C.; Chan, C. K. Water Content and Phase Transitions in Particles of Inorganic and Organic Species and their Mixtures Using Micro-Raman Spectroscopy. *Aerosol Sci. Technol.* **2010**, *44*, 269−280.
(36) Chu, Y.; Chan, C. K. Reactive Uptake of Dimethylamine by Ammonium Sulfate Ammonium Sulfate-Sucrose Mixed Particles. *J. Phys. Chem. A* **2017**, *121*, 206−215.
(37) Richards, D.; Trobaugh, K.; Hajek-Herrera, J.; Price, C. L.; Sheldon, C. S.; Davies, J. F.; Davis, R. D. Ion-Molecule Interactions Enable Unexpected Phase Transitions in Organic-Inorganic Aerosol. *Sci. Adv.* **2020**, *6*, No. eabb5643.
(38) Clegg, S. L.; Brimblecombe, P.; Wexler, A. S. Thermodynamic Model of the System $H^+$ - $NH4^+$ - $Na^+$ - $SO4^{2-}$ - $NO3^-$ - $Cl^-$ - H2O at 298.15 K. *J. Phys. Chem. A* **1998**, *102*, 2155−2171.
(39) Marcolli, C.; Krieger, U. Phase Changes during Hygroscopic Cycles of Mixed Organic/Inorganic Model Systems of Tropospheric Aerosols. *J. Phys. Chem. A* **2006**, *110*, 1881−1893.
(40) Han, F.; Zhang, J.; Chen, G.; Wei, X. Density, Viscosity, and Excess Properties for Aqueous Poly(ethylene glycol) Solution from (298.15 to 323.15) K. *J. Chem. Eng. Data* **2008**, *53*, 2598−2601.
(41) Jerome, F. S.; Tseng, J. T.; Fan, L. T. Viscosities of Aqueous Glycol Solutions. *J. Chem. Eng. Data* **1968**, *13*, 496.
(42) Grayson, J. W.; Evoy, E.; Song, M.; Chu, Y.; Maclean, A.; Nguyen, A.; Upshur, M. A.; Ebrahimi, M.; Chan, C. K.; Geiger, F. M.; et al. The Effect of Hydroxyl Functional Groups and Molar Mass on the Viscosities of Non-Crystalline Organic and Organic-Water Particles. *Atmos. Chem. Phys.* **2017**, *17*, 8509−8524.
(43) Marcus, Y. Ionic Radii in Aqueous Solutions. *Chem. Rev.* **1988**, *88*, 1475−1498.
(44) Price, H.; Mattsson, J.; Murray, B. Sucrose Diffusion in Aqueous Solution. *Phys. Chem. Chem. Phys.* **2016**, *18*, 19207−19216.
(45) Sidey, V. On the Effective Ionic Radii for Ammonium. *Acta Crystallogr., Sect. B: Struct. Sci., Cryst. Eng. Mater.* **2016**, *B72*, 626−633.
(46) Jimenez, J. L.; Canagaratna, M. R.; Donahue, N. M.; Prevot, A. S. H.; Zhang, Q.; Kroll, J. H.; DeCarlo, P. F.; Allan, J. D.; Coe, H.; Ng, N. L.; et al. Evolution of Organic Aerosols in the Atmosphere. *Science* **2009**, *326*, 1525−1529.
(47) Järvinen, E.; Ignatius, K.; Nichman, L.; Kristensen, T. B.; Fuchs, C.; Hoyle, C. R.; Höppel, N.; Corbin, J. C.; Craven, J.; Duplissy, J.; et al. Observation of Viscosity Transition in $\alpha$-pinene Secondary Organic Aerosol. *Atmos. Chem. Phys.* **2016**, *16*, 4423−4438.
(48) Cziczo, D. J.; Abbatt, J. P. D. Deliquescence, Efflorescence, and Supercooling of Ammonium Sulfate Aerosols at Low Temperature: Implications for Cirrus Cloud Formation and Aerosol Phase in the Atmosphere. *J. Geophys. Res.* **1999**, *104*, 13781−13790.
(49) Peckhaus, A.; Kiselev, A.; Wagner, R.; Duft, D.; Leisner, T. Temperature-dependent Formation of NaCl Dihydrate in Levitated NaCl and Sea Salt Aerosols Particles. *J. Chem. Phys.* **2016**, *145*, No. 244503.
(50) Wise, M. E.; Baustian, K. J.; Koop, T.; Freedman, M. A.; Jensen, E. J.; Tolbert, M. A. Depositional Ice Nucleation Onto Crystalline Hydrated NaCl Particles: a New Mechanism for Ice Formation in the Troposphere. *Atmos. Chem. Phys.* **2012**, *12*, 1121−1134.


https://doi.org/10.1021/acs.jpca.1c04471
J. Phys. Chem. A 2021, 125, 8668−8679